Developmental Cell, Vol. 8, 925–935, June, 2005, Copyright ©2005 by Elsevier Inc. DOI 10.1016/j.devcel.2005.03.011

Preferential Adhesion Mediated by Hibris and Roughest Regulates Morphogenesis and Patterning in the *Drosophila* Eye

Sujin Bao and Ross Cagan*
Department of Molecular Biology and Pharmacology
Washington University School of Medicine
660 South Euclid Avenue
St. Louis, Missouri 63110

Summary

Cell adhesion is essential for morphogenesis; however, the mechanisms by which cell adhesion coordinates precisely regulated morphogenesis are poorly understood. Here we analyze the morphogenetic processes that organize the interommatidial precursor cells (IPCs) of the *Drosophila* pupal eye. We demonstrate that the *Drosophila* immunoglobulin superfamily members Hibris and Roughest are essential for IPC morphogenesis in the eye. The two loci are expressed in complementary cell types, and Hibris and Roughest proteins bind directly in vivo. Primary pigment cells employ Hibris to function as organizers in this process; IPCs minimize contacts with neighboring IPCs and utilize Roughest to maximize contacts with primaries. In addition, we provide evidence that interactions between Hibris and Roughest promote junction formation and that levels of Roughest in individual cells determine their capacity for competition. Our results demonstrate that preferential adhesion mediated by heterophilic interacting cell-adhesion molecules can create a precise pattern by minimizing surface free energy.

Introduction

Morphogenesis is a fundamental developmental process by which individual cells are assembled into complex tissues and organs by means of cell shape change, cell movement, and controlled cell proliferation and cell death (reviewed in Schock and Perrimon, 2002). Cell adhesion is an essential component of morphogenesis. Multiple classes of cell-surface molecules are involved in mediating cell-cell and cell-matrix adhesion, and a number of models have been proposed that seek to explain how adhesion can influence cell fates and tissue patterning. These models have relied on relative binding affinities, cell sorting, etc. For example, Holtfreter demonstrated that reaggregation of dissociated amphibian embryonic cells led to a re-sorting of cells with their proper associative neighbors and often in their normal relative positions (Holtfreter, 1939; Holtfreter, 1944). Similar reaggregation studies led Steinberg to put forward the "differential adhesion hypothesis" (Steinberg, 1963; Steinberg, 1970), which proposed that sorting out of intermixed embryonic cells and envelopment of one embryonic tissue by another are driven by tissue interfacial free energies arising from cell adhesion. For example, differences in numbers of identical cell-adhesion molecules are sufficient to cause cell sorting and tissue spreading (Steinberg and Takeichi, 1994). This model emphasizes the principle of "self-organization" or "self-assembly": differential adhesion drives different cell populations to segregate from each other and organize them into patterning by minimizing adhesive free energy. Examples can be seen in the developing *Drosophila* wing, where differential adhesion segregates anterior/posterior and dorsal/ventral cells (e.g., Janody et al., 2003; Milan et al., 2001), and in the developing *Drosophila* eye, where cone cells segregate away from their neighbors and coalesce into simple patterns based on cadherin-mediated adhesion (Hayashi and Carthew, 2004).

The simplicity of the developing *Drosophila* eye has made it an especially useful model for studying epithelial morphogenesis. The compound eye derives from a monolayer columnar epithelium, the eye disc, which begins invagination during embryogenesis (Garcia-Bellido and Merriam, 1969). The eye disc remains proliferative and unpatterned until late in larval life, when a wave of differentiation generates a loosely arranged array of "unit eyes" or "ommatidia." Completed in the young pupa, these ommatidia are composed of eight photoreceptor cells, four lens-secreting cone cells, and two primary pigment cells (1°s; reviewed in Ready, 1989). As a last step, the pool of undifferentiated cells found between the ommatidial clusters—the interommatidial precursor cells (IPCs)—undergoes morphogenetic movements that eventually create a precise pigment cell lattice (Figures 1G and 1G′; Cagan and Ready, 1989). The function of this interommatidial lattice is to organize and optically insulate the ommatidial array. This final patterning process includes carefully regulated cell shape changes, cell movements, and cell death (reviewed in Rusconi et al., 2000). Although the processes that achieve this pattern are poorly understood, it is known to require *roughest*. The *roughest* locus encodes the Neph1 family member Roughest (Ramos et al., 1993), a protein that is essential for development of several structures including the eye. Mutations that abrogate *roughest* function lead to abnormally patterned ("rough") eyes and defects in the axons that target from eye to brain (Boschert et al., 1990; Ramos et al., 1993; Wolff and Ready, 1991). Cell culture experiments have led to the suggestion that Roughest may act through homophilic interactions (Schneider et al., 1995). This suggests that adhesion may play a role in directing IPC patterning, although the mechanisms have not been explored and the particular role of Roughest in the patterning process is not clear.

Neph1 and Nephrin proteins are members of the immunoglobulin superfamily, which includes transmembrane proteins that mediate Ca^{2+}-independent cell-cell adhesion (Barclay, 2003; Hynes and Lander, 1992). Recent years have seen a growing interest in Neph/Nephrin proteins, as they are dynamically expressed and are active in a wide variety of developmental pro-

*Correspondence: cagan@wustl.edu

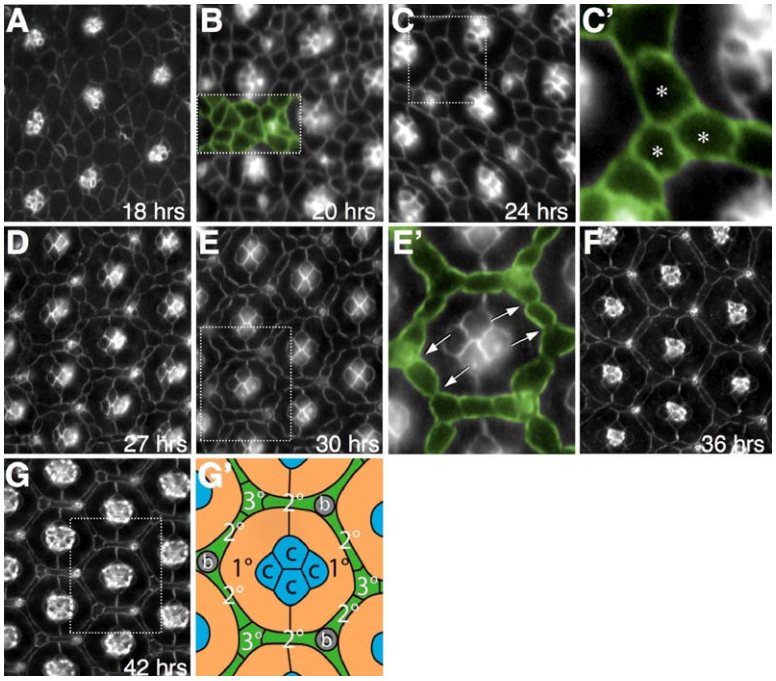

Figure 1. Interommatidial Precursor Cells Undergo Dynamic Cell Rearrangements in the Pupal Eye

Pupal eyes were stained with α-Armadillo antibody. Stages are as indicated (A–G). Armadillo levels are significantly lower in the IPCs (see text), and the overall contrast levels were increased to permit their visualization. (B) Boxed area contains IPCs that are artificially colorized to emphasize the multiple layers of IPCs between ommatidia at this stage. (C′) and (E′) are similarly colorized, expanded views of the boxed areas in (C) and (E), respectively: (C′) shows three cells positioned at a 3° vertex, and (E′) shows the scalloping at the IPC:1° border (arrows) that is typical for this stage. See text for details. (G′) Schematic representation of one 42 hr APF ommatidium traced from boxed ommatidium in (G). Abbreviations: c, cone cell; 1°, primary pigment cell; 2°, secondary pigment cell; 3°, tertiary pigment cell; and b, bristle group. Anterior is toward the right in this and all subsequent figures.

cesses in *C. elegans*, *Drosophila*, and mammals. These proteins contain a variable number of immunoglobulin repeats in their extracellular domain. In mammals, both heterophilic and homophilic interactions of Neph1/Nephrin proteins have been proposed (Barletta et al., 2003; Donoviel et al., 2001; Gerke et al., 2003; Khoshnoodi et al., 2003; Liu et al., 2003; Sellin et al., 2003). However, the mechanisms by which Neph1/Nephrin proteins function in vivo, e.g., during mammalian kidney development, remain unclear. Recently, it has been demonstrated that heterophilic interactions between SYG-1 and SYG-2, two Neph1/Nephrin homologs in *C. elegans*, determine the specificity of synapse formation (Shen and Bargmann, 2003; Shen et al., 2004). In *Drosophila*, in addition to Roughest, one Neph1 homolog (Kirre) and two Nephrin homologs (Sticks-and-stones and Hibris) have been identified (Artero et al., 2001; Bour et al., 2000; Dworak et al., 2001; Strunkelnberg et al., 2001). The mechanisms by which these transmembrane proteins direct development are not clear.

To gain further insight on how cell adhesion molecules coordinate cell adhesion and morphogenesis, we explored the roles of Hibris and Roughest during IPC morphogenesis. We demonstrate that Hibris functions as a Roughest binding protein in the pupal eye. This binding is used by 1°s to organize the morphogenesis and patterning of IPCs into a hexagonal lattice. IPCs maximize contact with 1°s and minimize contact with neighboring IPCs; we provide evidence that this preferential adhesion of IPCs to 1°s is mediated by interactions between Hibris and Roughest. Our results indicate how this process can use cell-cell adhesion, properly and dynamically regulated, to lead to the emergence of a precise cell pattern within a developing epithelium.

Results

Interommatidial Precursor Cells Undergo Dynamic Morphogenetic Movement in the Pupal Eye

To properly organize the ommatidia into a precise pattern, the interommatidial precursor cells (IPCs) undergo dynamic cell rearrangements between 18 and 42 hr after puparium formation (APF). These cells will eventually differentiate as secondary and tertiary pigment cells (2°s, 3°s) and mechanosensory bristles (Figures 1G and 1G′). We further examined emergence of the interommatidial lattice with an antibody to the β-catenin ortholog Armadillo (Arm), a core component of the adherens junction. Representative panels from eyes aged 18–42 hr APF are presented in Figure 1. Based on this work, we classify IPC and ommatidial patterning into four stages (hours are based on the approximate center of the eye field), which are briefly described.

(1) Initial cell sorting (18–24 hr APF). Initially, IPCs are scattered between ommatidia with a relaxed apical profile (Figure 1A). As development progresses, two cells emerge from the IPC pool to enwrap the cone cells and become 1°s; the remaining IPCs simultaneously line up in single file to contact 1°s from adjacent ommatidia (Figures 1B–1C′; Cagan and Ready, 1989; Reiter et al., 1996). Concurrently, some cells are removed by apoptosis (Rusconi et al., 2000).

(2) Emergence of 3°s (24–27 hr APF). Typically, three cells are initially positioned equally at a vertex. One cell reaches past the other two to contact a third 1°; this cell will then physically "invade" the vertex and mature as a 3° (Figure 1D).

(3) Selection of 2°s (27–36 hr APF). Cells that fail to become 3°s either become 2°s or are removed by programmed cell death (Figures 1D–1F). During this final

cell-fate decision, cell-cell adhesion becomes visibly polarized as IPCs form detectable junctional contacts with 1°s but not with other IPCs. In addition, we observed a "scalloping" of membrane profiles as 1°s push between IPCs, further confirming that the adhesion between 1°s and IPCs are greater than between neighboring IPCs (Figures 1D and 1E). By 36 hr APF, the hexagonal pattern is essentially complete: it is composed of a single 2° at each side and a 3° or bristle organule at each vertex (Figure 1F).

(4) Maturation (36–42 hr APF). Visible adherens junctions return to the interfaces between IPCs (now 2°s and 3°s). Contacts are now smoothed as the scalloping caused by invasive 1° contacts is relaxed (Figures 1G and 1G′).

One particularly striking feature of this morphogenetic process is the dynamic nature of the cell junctions, which was visualized with the junctional protein Arm. For example, the level of Arm in the cone cells was constant but the levels of Arm in the IPCs decreased: this was seen by comparing the levels of Arm in the two cell groups (Figures 1B and 1C). This drop in Arm levels is followed by its complete loss between IPCs after 3°s emerge (Figures 1D–1F) and eventual reemergence at the final maturation stage to levels similar to cone cells (Figure 1G). Thus, junctions appear to be diminished during the period of maximal cell rearrangement, suggesting that IPCs are free to move during these stages.

Abnormal Morphogenetic Movements in *hibris* and *roughest* Mutants

Previous studies demonstrated that overexpression of Hibris can lead to disrupted development of adult tissues including the eye (Dworak et al., 2001). Reducing *hibris* activity led to early defects in ommatidial development, including abnormal configurations of photoreceptors and cone cells (see Supplemental Figure S1 available with this article online), abnormal arrangements of the cone cell quartet, and ommatidial fusions. To determine the effects of reducing *hibris* activity specifically during the stage in which IPCs are reorganized in the pupal eye, transgenic flies were generated containing an RNAi construct that specifically inhibited *hibris* expression through inverted repeat-mediated RNA interference (*hibris-IR*; see Experimental Procedures). This construct was driven with the eye-specific promoter *GMR-GAL4* (Moses and Rubin, 1991) to direct reduction of *hibris* levels to the late larval and early pupal eye. Assembly of the ommatidial cores in developing *GMR>hibris-IR* eyes was largely unaffected; occasional failure of cone cells to form a proper quartet was observed (data not shown). At 24 hr APF (the initial cell-sorting stage) when IPCs normally reorganize to lie single-file around the 1°s, *GMR>hibris-IR* mutant eyes contained IPCs that failed to properly sort into a single line (Figure 2D). IPCs had abnormally "relaxed" cell morphologies, failing to maximize their contacts with 1°s (scalloping) or reduce their contacts with neighboring IPCs (Figure 2E). In addition, bristle groups were often either missing or misplaced; their placement is dependent on proper IPC morphogenesis (Cagan and Ready, 1989). 3°s were especially affected: at 30 hr APF, the 2–3 cells that normally compete to establish a single 3° at vertices commonly failed to resolve to a single 3° (Figure 2E). In approximately two-thirds of *GMR>hibris-IR* vertices, 2–3 cells were observed to occupy the vertex position, none successfully contacting three 1°s (Figure 2F). To accommodate these cells—or perhaps due to more direct effects of reducing *hibris*—the apical profiles of 2°s were often smaller (Figure 2F). These patterning defects led to ommatidial misalignment and a rough eye phenotype in the adult (Figure 2B).

A more extreme example of a failure of IPCs to properly assemble into a hexagonal pattern can be found in the eyes containing a strong loss-of-function mutation in the *roughest* locus. The mutant allele $rough^{CT}$ encodes a truncated Roughest protein that affects protein localization and strongly reduces function in the developing eye (Ramos et al., 1993; Reiter et al., 1996; Wolff and Ready, 1991). In a 24 hr APF $rough^{CT}$ eye, ommatidial cores were formed normally but IPCs failed to sort into a single line; subsequent patterning steps were arrested (Figure 2G; Reiter et al., 1996). Within vertices of more mature eyes, three or more cells often shared a 3° niche, and bristle groups failed to move into their proper positions. These failures of cellular rearrangement were also accompanied by abnormal apical morphologies: at 30 hr APF, IPCs had unusually large apical profiles that failed to form the typical scalloped contacts with 1°s or minimize contacts with neighboring IPCs (Figure 2H). Polarized cell-cell adhesion was disrupted and uniform levels of Armadillo were observed at IPC:IPC and 1°:IPC borders. These failures of proper cell morphogenesis led to a disrupted interommatidial lattice composed of IPCs that have not properly organized into a hexagon but instead lie side by side. The result is a rough adult eye phenotype that is due to disorganized rows of ommatidia (Figure 2I).

hibris and *roughest* Are Expressed in Complementary Cell Types

Nephrin and Neph1 family members have been linked in other developing systems (Barletta et al., 2003; Gerke et al., 2003; Liu et al., 2003) and, given their similar effects on IPC maturation, we further explored associations between these two transmembrane proteins. The P element insertion line P[w+]36.1 is an "enhancer trap" that faithfully reports *hibris* expression (Artero et al., 2001). Hibris is expressed at late larval stages of eye development (Dworak et al., 2001). In the young pupa, expression of *hibris* was observed in cone cells and 1°s at 24 hr and 30 hr APF (Figures 3A and 3B); low-level *hibris* expression was also detected in photoreceptor cells. We did not detect expression in IPCs. This pattern of expression was unchanged until at least 42 hr APF (data not shown). In contrast, Roughest exhibits dynamic expression from larval through pupal development (Reiter et al., 1996). High levels of Roughest protein were found at the border between 1°s and IPCs at 24 hr APF as assessed with a Roughest-specific antibody (Figure 3D; Reiter et al., 1996). Substantially lower levels of protein were detected at the contacting surface between two 1°s and at the borders between neighboring IPCs. In situ hybridization con-

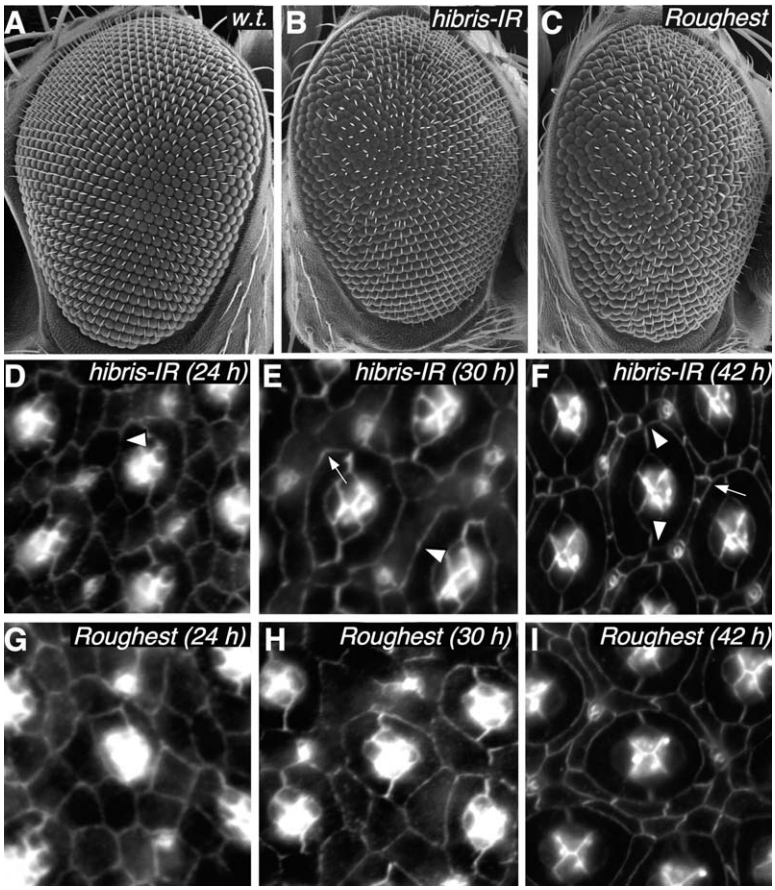

Figure 2. Abnormal Morphogenetic Movement in *hibris* and *roughest* Mutants

(A–C) Scanning electron micrographs of adult eyes from wild-type (A), *hibris-IR* (B), and *roughest*^{CT} (C).

(D–I) Pupal eyes stained with α-Armadillo.

(D–F) *hibris-IR* at 24 hr APF (D), 30 hr APF (E), and 42 hr APF (F).

(D) An arrowhead points to two layers of IPCs that failed to line up in single file.

(E) The arrowhead indicates an abnormally straight border between IPCs and a 1°. Also, scalloping is reduced at IPC:1° contacts, and IPC:IPC contacts are not minimized (compare with Figure 1E′). An arrow points to three cells that fail to resolve to a single 3°.

(F) Arrowheads show examples of reduced apical profiles of 2°s and the arrow points to a niche that has failed to resolve to a single 3°.

(G–I) *roughest*^{CT} pupal eyes at 24 hr APF (G), 30 hr APF (H), and 42 hr APF (I). IPCs failed to line up in single file (D); subsequent patterning steps were arrested (see text for details).

firmed that *roughest* mRNA was found predominantly within the IPCs at 24 hr APF (Figure 3C). By 30 hr APF, as the IPCs are actively rearranging, detectable protein disappeared at the borders between IPCs (Figure 3E), a localization pattern strikingly reminiscent of the loss of Armadillo and DE-cadherin at the same developmental stages. In fact, Roughest, Armadillo, and DE-cadherin precisely colocalized along IPC borders at this later stage (see below). This targeting of Roughest protein was retained until at least 42 hr APF (Figure 3F). Roughest protein in IPCs was also observed at high levels within apical vesicles at all stages (Figures 3D and 3E; Reiter et al., 1996).

Hibris Functions as a Roughest Binding Protein

To determine if *hibris* and *roughest* activities are functionally linked in the retina, we assessed each gene's ability to genetically modify the other's activity in situ; previous overexpression studies failed to identify such an interaction (Dworak et al., 2001). First, we determined that *roughest*^{CT} alleles had a mild dominant effect in the pupal eye that predominantly affected 3° specification: in genotypically *roughest*^{CT}/+ heterozygous 42 hr APF females, cell rearrangement defects were observed in 17% of 3° niches (n = 240 ommatidia from 5 animals). Most commonly, two cells occupied one 3° niche (Figure 4A), a phenotype reminiscent of

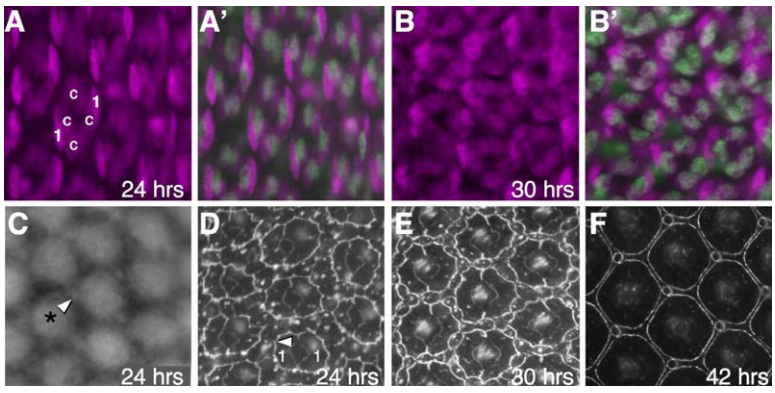

Figure 3. *hibris* and *roughest* Are Expressed in Complementary Cell Types

(A–B′) *hibris* expression was visualized with the *P[w+]36.1* reporter and anti-β-galactosidase antibody (magenta); costained with the cone cell marker Cut (green, [A′] and [B′]). c, cone cell; 1, primary pigment cell.

(C) An in situ hybridization of *roughest*. Asterisk highlights the center of one ommatidium while arrowhead indicates a (unstained) bristle group.

(D–F) Pupal eyes that were stained with α-Roughest antibody at the stages indicated. Roughest protein predominantly accumulated in the border between IPCs and 1°s (arrowhead highlights an example); "1"s indicate two 1°s (D). See text for details.

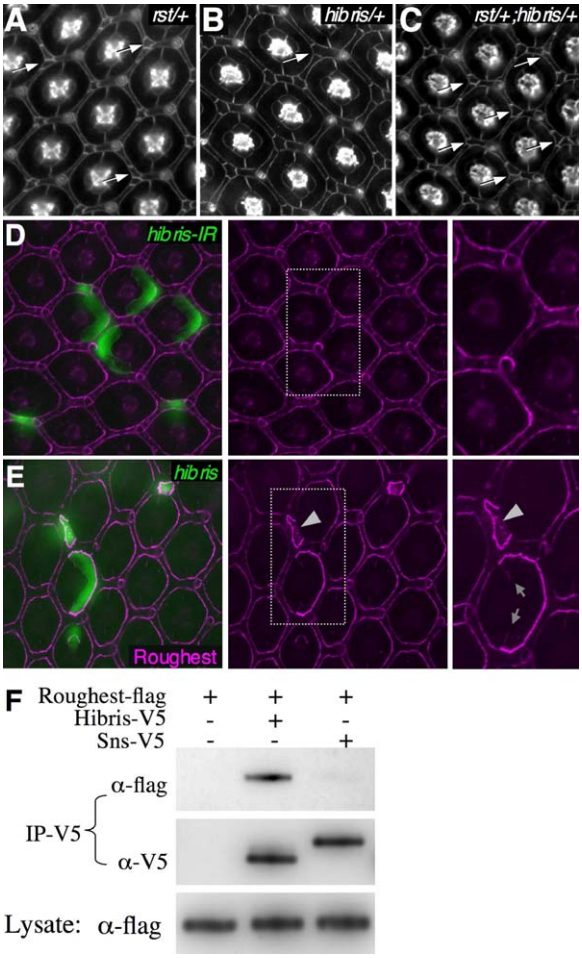

Figure 4. Hibris Functions as a Roughest Binding Protein

(A–C) *hibris* interacts genetically with *roughest*. Arrows highlight defects.

(A) *roughest*^{CT} (*rst*) showed a mild dominant effect in the interommatidial lattice that predominantly affected 3° specification.

(B) *hibris* is fully recessive (other than occasional misplaced or missing bristle organules).

(C) Removing a single functional copy of *hibris* (*roughest*^{CT}/+; *hibris*^{459}/+) showed an enhanced penetrance of 3° defects compared to *roughest*^{CT}/+ alone.

(D) Downregulation of *hibris* activity in FLP-out clones utilizing *hibris-IR*. Clones were marked by GFP (green). Roughest protein (magenta) was significantly reduced in IPCs adjacent to *hibris-IR* 1°s. The right panel shows an enlarged view of boxed region in left panel.

(E) Overexpressing *hibris* in FLP-out clones. Clones were marked by GFP (green). Roughest protein (magenta) was significantly increased next to *hibris* 1°s. Enlarged view of boxed region is shown in the right panel. High levels of Hibris in a 1° led to its expansion at the expense of the neighboring 1° (arrows). An IPC with high levels of Hibris was recognized as part of the neighboring complement of 1°s (arrowhead).

(F) Roughest protein coimmunoprecipitated with Hibris (middle lane). In contrast, very little Roughest protein was coimmunoprecipitated with Sticks-and-stones (Sns; right lane).

the defects observed at the vertices of *GMR>hibris-IR* eyes (Figure 2F). Less commonly, we observed examples of a single 3° precursor cell that failed to fully exclude the neighboring two 2°s. Although *hibris* alone was found to be essentially fully recessive (with the exception of occasional misplaced or missing bristles; Figure 4B), additional removal of a single functional copy of *hibris* (*roughest*^{CT}/+;*hibris*^{459}/+) increased the incidence of abnormal vertices to 37% (n = 255 ommatidia from 5 animals; Figure 4C). In addition, some vertices failed to contain any 3°s, bristles were occasionally missing, and some 2°s had abnormal morphologies. Together, our data indicate that *hibris* and *roughest* are functionally linked as they direct morphogenetic movement of cells within the interommatidial lattice.

The preferential accumulation of Roughest protein at the border between 1°s and IPCs suggested the presence of an interacting partner protein expressed in 1°s that attracted Roughest protein. Our genetic data suggested Hibris as a candidate. To test this possibility, we utilized FLP-out technology (Basler and Struhl, 1994) to assess the effects of reducing or increasing *hibris* in individual 1° cells. Reducing Hibris expression by expressing *hibris-IR* in individual 1°s led to a consistent and significant reduction in Roughest protein level in IPCs positioned at the border adjacent to the *hibris-IR* clones (Figure 4D). Conversely, when wild-type Hibris was overexpressed in individual 1°s, Roughest protein levels markedly increased in neighboring IPCs; this increase occurred exclusively at the portion of the IPC border in direct contact with the ectopic Hibris-expressing 1° (Figure 4E). Similarly, expressing ectopic Hibris in cone cells led to local accumulation of Roughest protein in neighboring 1°s (Figure 4E), indicating that the presence of Hibris is sufficient to attract Roughest regardless of the cell's identity. Similar experiments that targeted overexpression of the Hibris paralog Sticks-and-stones (Bour et al., 2000) to the 1°s did not affect Roughest localization (data not shown), suggesting that Sticks-and-stones and Roughest do not form a complex in situ. Consistent with this view, Sticks-and-stones failed to demonstrate significant binding to Roughest in immunoprecipitation studies (see below).

Overexpressing Hibris in individual cells had informative patterning consequences as well. For example, artificially high levels of Hibris within a 1° led to its small but reproducible expansion at the expense of its partner 1° (Figure 4E). IPCs that expressed ectopic Hibris presented with two striking defects. Creating overexpression clones of Hibris late (e.g., 18 hr APF) led to a fairly small apical profile and exclusion from the flow of the interommatidial lattice. In these examples, the lattice was typically built correctly around the cell, indicating that the Hibris-expressing IPC was recognized as part of the neighboring complement of 1°s and that the presence of a contiguous band of Hibris was itself sufficient to organize the interommatidial lattice regardless of the number of 1°s providing it. That is, the presence of Hibris alone is sufficient to provide a cell with 1°-like organizing activity (Figure 4E). The other predominant phenotype was observed in Hibris overexpression clones that were created early (e.g., 3 hr APF) in single IPCs. These cells typically had an abnormally large border with neighboring IPCs, and this border contained abnormally high levels of Roughest and the junctional protein DE-cadherin (Figure 5E). Together, these data indicate that Hibris can associate with Roughest in

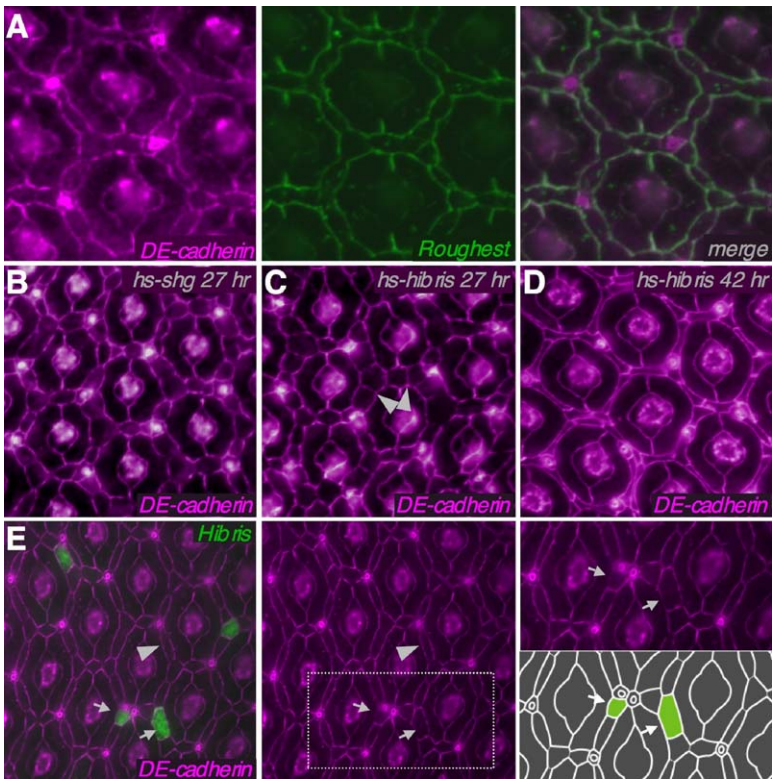

Figure 5. Interaction between Hibris and Roughest Promotes Junction Formation

(A) Roughest (green) colocalizes with DE-cadherin (magenta) in a 30 hr APF pupal eye. Merged image is shown in the right panel.

(B–D) Pupae at 25.5 hr APF were heat-shocked for 25 min at 37°C and dissected at 27 hr (B and C) or 42 hr (D). (B) Ubiquitous expression of DE-cadherin did not alter polarized cell junctions. (C) In contrast, ubiquitous expression of Hibris disrupted polarized cell junctions. Straight borders formed between IPCs by 1 hr 30 min after induction of Hibris expression by heat shock (arrowheads), leading to rough eye phenotype (D).

(E) Ectopic expression of *hibris* in FLP-out clones. Clones were induced at 6 hr APF and marked by GFP (green, left panel). The pupal eye at 36 hr APF was stained with anti-DE-cadherin antibody (magenta, left and middle panels). IPCs with ectopic *hibris* formed a DE-cadherin-rich border with neighboring IPCs. Each clone formed a straight border with its neighboring IPC (arrow) while control IPCs formed minimally detectable adherens junctions (arrowhead). Enlarged view of boxed region in middle column is shown in the right; a tracing is also provided for clarity.

trans across cell borders and that Hibris provides important patterning and junctional information required to organize the hexagonal pattern.

To assess whether Hibris can associate directly with Roughest, we performed a coimmunoprecipitation assay. Hibris and Roughest proteins were followed by the addition of a C-terminal V5 and FLAG tag, respectively. Hibris- and Roughest-transfected *Drosophila* S2 cells were cocultured and the mixed cells were lysed. Roughest protein was coimmunoprecipitated with Hibris from the cell lysate (Figure 4F). Conversely, immunoprecipitation of Roughest led to coimmunoprecipitation of Hibris (data not shown). Although we cannot rule out additional intermediates that may be required for Hibris-Roughest association, our data strongly suggest that Hibris interacts directly with Roughest in the pupal eye and that this interaction is required for important aspects of the patterning process.

Interactions between Hibris and Roughest Promote Junction Formation

In order for morphogenesis to proceed correctly, cell junctions should be tightly regulated. As described above, by the stage that 3°s are being selected (27 hr APF), cell junctions are polarized: IPCs establish elaborate cell junctions with 1°s but minimal junctions with their neighboring IPCs. Roughest has a similar polarized distribution at this stage, and, interestingly, it colocalizes with adherens junctions (Figure 5A). These data suggest a link between Hibris/Roughest interactions and junction formation.

Ubiquitous expression of DE-Cadherin did not change polarized cell junctions (Figure 5B), indicating that high levels of DE-Cadherin alone are not sufficient to create cell junctions between IPCs. In contrast, ubiquitous expression of Hibris disrupted the polarized pattern of cell junctions (Figure 5C). To explore its role in regulating junction formation at a finer level, we used ectopic expression of Hibris in single cells. Individual IPCs that received ectopic Hibris formed a DE-Cadherin-rich border with neighboring IPCs that was sharp, straight, and significantly enlarged (Figure 5E). In addition, ectopic septate junctions were also detected using the marker Discs Large (data not shown). Again, ectopic cell junctions were not observed in single cells overexpressing DE-Cadherin (data not shown). Taken together, these data strongly suggest that the presence of a Hibris/Roughest border is sufficient to establish or stabilize a stable and robust junction between cells. Therefore, as a binding pair, Hibris and Roughest promote junction formation. However, it is worth noting that interactions between Hibris and Roughest are not absolutely required to establish cell junctions: in eyes mutant for the severe allele *roughest*^{CT}, cell junctions still formed between IPCs and 1°s, although the normal polarization of junctional proteins was lost (Figures 2G–2I).

Levels of Roughest Alter Cell-Cell Competition

Finally, to better understand the links between Roughest and patterning, we utilized FLP-out techniques to alter the protein level of Roughest in individual IPCs at the beginning of the patterning process. We targeted individual IPCs utilizing an inverted-repeat construct that reduced *roughest* mRNA levels (*roughest-IR*; see

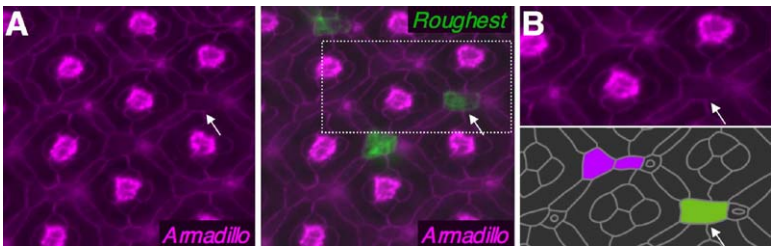

Figure 6. Levels of *roughest* Alter Cell Competition

(A) Ectopic expression of *roughest* in FLP-out clones. Clones were induced at 6 hr APF and marked by GFP (green); cells were marked with α-Armadillo (magenta). In 39 hr APF pupal eyes, IPCs receiving ectopic *roughest* (arrow) underwent expansion, leading to a removal of neighboring IPCs that permitted a normally spaced lattice.

(B) Enlarged view of boxed region in previous panel; in the matched tracing, a cell with ectopic Hibris is highlighted in green and a normal 2°/3° pair is marked in magenta.

Experimental Procedures). Cells with reduced *roughest* activity were marked by GFP. In a 42 hr APF wild-type eye field, the ratio between the number of 2°/3°s versus 1°s (IPC:1°) is 2:1. In a control experiment where only GFP was ectopically expressed, the ratio of GFP-expressing IPCs to 1°s was 1.88:1 (n = 440 clones, 10 eyes). In contrast, targeting *roughest-IR* to individual cells led to an IPC:1° ratio of 0.97:1 (n = 837, 24 eyes). This difference indicates that reducing *roughest* activity in an IPC rendered the cell less competitive in the process of selecting 2°s or 3°s. It further highlights the important role that Roughest plays in directing IPCs into the hexagonal pattern.

Finally, we further tested the importance of Roughest in directing IPC patterning by utilizing FLP-out technology to similarly target ectopic Roughest to individual cells. The result was striking: ectopic Roughest within an IPC led to significant and stable expansion of its apical profile. Typically, these cells expanded to include both the 2° and the 3° niche, i.e., a single cell took over two cell niches. These "hybrid" 2°/3° cells contacted five 1°s and, remarkably, maintained the correct positioning and spacing of a 2° plus a 3° (Figures 6A and 6B). At this late stage, the expansion of the cell was coupled with a normal level of DE-cadherin protein along the IPC:1° border, indicating that the levels of DE-cadherin expanded to accommodate the increased cell size. Additional cells were not relocated to neighboring niches but were instead lost, presumably through ectopic programmed cell death. Similar to our experiments with ectopic Hibris, these data indicate that IPC patterning refers to the amount of Roughest and not the number of cells expressing it. They also indicate that levels of Roughest in individual cells may determine their capacity for competing for specific cell niches in the interommatidial lattice.

Discussion

Using laser ablation studies, we previously demonstrated that 1°s are centrally important for the process of organizing IPCs into a correctly patterned interommatidial lattice (Miller and Cagan, 1998). However, the mechanism by which one cell can provide such remarkably precise patterning information to a larger collection of uncommitted cells was not clear. The dynamic interactions between Hibris and Roughest provide such a mechanism.

Differential Adhesion and Morphogenesis

The "differential adhesion hypothesis" (DAH) proposed that sorting-out and segregation of cell populations are driven by differences in the intensities of cell adhesions (Steinberg, 1963; Steinberg, 1970). Given motile and cohesive cell populations, DAH predicts that weakly cohesive cells will tend to be displaced by more strongly cohesive ones; this process can direct cells to segregate away from unlike cell populations, and it can control tissue spreading during, for example, germ layer maturation in the embryo. DAH has been supported by several observations. For example, quantitative differences in the level of cadherin expression can lead two cell populations to be mutually immiscible: less cohesive cells will envelope more cohesive ones, creating a "sphere within a sphere" configuration (Steinberg and Takeichi, 1994). Recently, the importance of differential adhesion for patterning developing tissue was demonstrated in the pupal retina. Hayashi and Carthew (2004) showed that cone cells segregate from other cells and assemble into a simple pattern by minimizing surface area as soap bubbles do. This assembly is mediated at least in part by E- and N-cadherins, and manipulating cadherin levels within the cone cells or their neighbors can alter the final cone cell pattern (Hayashi and Carthew, 2004). These experiments illustrate that differential adhesion caused by differences in cadherin expression can mediate morphogenesis and pattern formation.

Our data indicate that IPC patterning follows a mechanism that shows unique aspects when compared with these classical DAH experiments. First, manipulating E-cadherin levels did not alter the morphogenesis or arrangement of IPCs (Figure 5B). Even when two neighboring IPCs have higher levels of E-cadherin, adhesion between these two IPCs or their final patterning is not affected (data not shown). More critically, IPCs do not aggregate together or segregate away from their neighbors. Rather, they *separate* away from each other to minimize IPC:IPC contacts, and *aggregate* with ommatidial cores to maximize 1°:IPC contacts. That is, our data indicate that IPCs have a preference for adherence to 1°s. This preference can be seen most clearly at 27 hr APF: the junctions between IPCs and 1°s are strong and elaborate, the junctions between IPCs are indistinct, and 1°s are seen to push between IPCs to maximize contact and create a scalloping effect (Figures 1D and 1E). The result is the precise aggregation of two different cell populations.

Hibris/Roughest and Preferential Adhesion

Why do IPCs sort away from other IPCs and preferentially adhere to 1°s? Our data indicate that interactions between Hibris and Roughest provide the mechanism.

Hibris and Roughest Mediate Heterophilic Interactions

The immunoglobulin-class proteins Roughest and Hibris are utilized by IPCs and 1°s, respectively, to form heterophilic interactions. Several lines of evidence support this view. First, both Hibris and Roughest are required for proper interommatidial lattice assembly. Second, *hibris* is expressed in 1°s as well as in cone cells and *roughest* is expressed in IPCs at the time of IPC rearrangement in the eye. Third, expression of ectopic Hibris in either the 1° or IPC was sufficient to relocalize Roughest protein. Conversely, downregulation of Hibris in 1°s led to decreased levels of Roughest protein at the 1°:IPC interface. Finally, Hibris and Roughest are capable of directly binding each other when isolated in tissue culture experiments.

Roughest Has Stronger In Vivo Affinity to Hibris than to Itself

After 1°s are specified and start to express Hibris, levels of Roughest protein decrease between IPCs and increase in the borders between IPCs and 1°s; for example, at 30 hr APF, Roughest protein is undetectable between IPCs (Figures 3D and 3E). Furthermore, ectopic Hibris in 1°s is sufficient to attract still more Roughest protein toward the 1°:IPC border (Figure 4E); by contrast, ectopic Roughest in 1°s does not attract additional Roughest (data not shown). We conclude that although Roughest can show homophilic interactions in S2 cells (Dworak et al., 2001; Schneider et al., 1995), it strongly prefers heterophilic interactions with Hibris in situ.

Interactions between Hibris and Roughest Promote Junction Formation

Ubiquitous Hibris expression greatly increased the levels of cell-junction proteins between IPCs (Figure 5C). Similarly, individual IPCs that received ectopic Hibris formed E-cadherin-rich borders with neighboring IPCs that were sharp, straight, and significantly enlarged (Figure 5E).

Our evidence indicates that 1°s and IPCs prefer to adhere to each other based on their expression of Hibris and Roughest, respectively. One principle of thermodynamics states that the binding of two adherent molecules will lead to a reduction of free energy within the system, provided the equilibrium constant of association (k_a) is greater than the equilibrium constant of dissociation (k_d) (Creighton, 1984). The essential role of Hibris and Roughest in IPC morphogenesis prompts us to make an assumption: among the various molecules being displayed in the surfaces of 1° s and IPCs, Hibris and Roughest play a major role in determining the flow of free energy. Roughest has a higher affinity for Hibris than itself, and therefore heterophilic binding between Roughest and Hibris leads to a greater reduction in free energy. As a result, contacts between IPCs and 1°s contribute to a reduction of free energy and are favored, while contacts between IPCs and IPCs do not contribute to reduction of free energy and are disfavored.

Other features of the developing pupal eye provide important components to this patterning process. After 1°s are specified, they establish cell junctions with each other and with cone cells. These cone cell/1° units are not free to move within the epithelial plane and form a functional patterning unit. Therefore, 1°s function as the organizers in this context. In contrast, IPCs have reduced levels of junctional proteins and are free to move within the epithelium (Figures 1B and 1C). Numerous filopodia from IPCs observed by SEM studies also point to their potential for high motility (Frohlich, 2001). Taken together, our data suggest that IPC morphogenesis follows a preferential adhesion model: IPCs exhibit preferential adhesion to 1°s; 1°s function as organizers for IPC morphogenesis; and IPC:1° contacts are free energy favored while IPC:IPC contacts are disfavored.

Preferential Adhesion Model and IPC Morphogenesis

The ommatidial clusters are poorly organized until 18 hr APF, when the morphogenetic movements of the IPCs begin to organize them into a hexagonal array. Preferential adhesion of IPCs to 1°s yields two major outcomes. First, IPCs compete to adhere directly to the limited, Hibris-rich surface presented by the 1°s. High motility of IPCs permits this competition to proceed and achieve a favored configuration. Second, preferential adhesion can also lead to the removal of cells that fail to contact a 1°. Specifically, IPCs that adhere to 1°s have an increased chance to survive since the Hibris:Roughest interactions provide a greater opportunity to establish a stable junction. By the same token, those cells that do not have access to 1°s are disadvantaged and are commonly dropped from the apical surface; these cells are likely to be eventually removed by programmed cell death. As a result, each stage proceeds with a progressive reduction of the IPC:IPC contacting surfaces and an increase in IPC:1° contacting surfaces.

At the onset of IPC morphogenesis (18 hr APF), the average size of IPC:IPC contacts is not significantly different from the size of IPC:1° contacts (Figure 7A). As cells in multiple layers are sorted into single file after the initial cell-sorting stage (24 hr APF; see above), IPC:IPC contacts are significantly reduced (Figure 7B). After emergence of 3°s, this reduction in IPC:IPC contacts is particularly dramatic. The IPC:1° contacts are increased by a scalloped profile, a further demonstration that IPC:IPC contacts are disfavored (Figure 7C). To complete this pattern, therefore, IPC:IPC contacts are further minimized by reducing the number of candidate 2°s to one cell between each 3° and bristle (Figure 7D). Thus, IPC morphogenesis reveals a mechanism by which pattern is determined through minimizing disfavored cell-cell contacts and maximizing preferred cell-cell contacts.

Finally, it is interesting to note how 2°s are selected. After emergence of 3°s, two IPCs are commonly found between a 3° and bristle. In many ways, these two IPCs are equal: each contacts two 1°s and each establishes equally strong cell junctions; each forms a scalloped contour with two neighboring 1°s; and each is exposed to the same molecular cues. However, we have provided evidence that these two cells have a low affinity for each other, a situation that is not favored by mini-

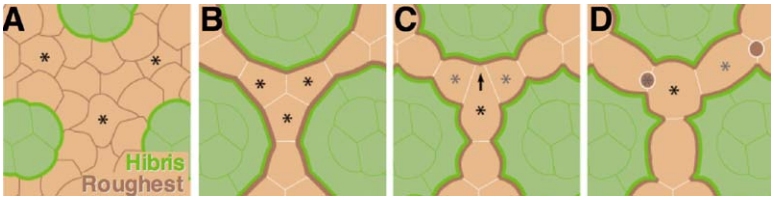

Figure 7. IPC Morphogenesis and Preferential Adhesion Model

IPCs are highlighted in orange to indicate Roughest expression, and 1°s and cone cells are marked in green to indicate Hibris expression. Three future 3° candidates are indicated by asterisks (the 3° candidates in [B] are assigned at random to emphasize the effects of cell movements).

(A) At the onset of IPC morphogenesis, multiple layers of cells are scattered between ommatidia, and low levels of cell junctions at IPC:IPC borders allow IPCs to move freely. The average size of contacts between all interommatidial cells (IPCs and future 1°s) are similar at this stage.

(B) After 1°s are specified, preferential adhesion mediated by Hibris and Roughest (thick green lines and brown lines) determine that IPC:1° contacts are free energy favored while IPC:IPC contact are disfavored. As a result, the size of IPC:IPC contacts is reduced and the size of the IPC:1° contacts is increased. Three 3° candidates compete for the single 3° niche (asterisks).

(C) After one candidate establishes stable cell junctions with a third 1°, the other two competing IPCs join other IPCs to compete for a 2° fate. As 3°s emerge, IPC:1° contacts become still more robust as reflected in the scalloping observed at IPC:1° contacts. Cell junctions are established between IPC:1° while cell junctions between IPC:IPC are undetectable.

(D) A single 2° is established at each hexagonal face as cell competition results in removal of all but one cell between each 3° and bristle group; levels of Roughest in individual cells may influence this choice. At this stage, the process of preferential adhesion yields minimized IPC:IPC contacts and maximized IPC:1° contacts. In this manner, a hexagonal pattern is determined by mechanisms that minimize disfavored contacts and maximize preferred contacts.

mum free energy principles. One cell will be removed. How is this cell chosen? Clues came from manipulating levels of Roughest, which altered each cell's capacity for competition. Artificially high levels of Roughest rendered a cell a supercompetitor: the targeted cell even replaced two cells to become both a 2° and a 3° (Figures 6A and 6B). Presumably, high levels of Roughest promote a higher level of cell junctions, which makes a cell more competitive and determines the survivor. Conversely, low levels of Roughest put the targeted cell at a disadvantage during this competition (see Results). Therefore, during the selection of a 2°, differing levels of Roughest expressed by each cell may determine its fate: survival or death.

Neph1/Nephrin family members are required for the development of a wide array of tissues including axonal pathfinding and myoblast fusion in *Drosophila* and formation of the slit diaphragm in the developing mammalian kidney. The role we observed for preferential adhesion in IPC morphogenesis and patterning in the *Drosophila* eye leads to the interesting possibility that similar mechanisms are utilized broadly in pattern formation.

Experimental Procedures

Fly Stocks

All crosses and staging were conducted at 25°C, except where noted. Stocks used were Canton-Special (wild-type), *hibris*^{459}, *hibris*^{2593}, and *hibris* reporter *P[w+]36.1* (Artero et al., 2001), *UAS-hibris* (Dworak et al., 2001), *UAS-roughest* (Reiter et al., 1996), and *UAS-DE-cadherin* (Sanson et al., 1996). RNA interference (inverted repeat) flies *UAS-hibris-IR* and *UAS-roughest-IR* were generated for this work. *roughest*^{CT}, *GMR-GAL4*, *hs-GAL4*, *actin5C-GAL4, white;Δ2-3*, and *P[act5C>y+>GAL4] P[UAS-GFP.S65.T]/CyO,y+* were provided by the Bloomington *Drosophila* Stock center.

Constructs and Germline Transformation

An additional *white* intron flanked by AvrII and NheI from *pWIZ* (Lee and Carthew, 2003) was engineered into XhoI/XbaI sites of *pGEM-T* (Promega) to create an intermediate vector *pGEM-WIZ* to assemble inverted repeats for RNA interference. To make *hibris* RNA interference construct *pUAS-hibris-IR*, *hibris* cDNA fragment 167–670 (Flybase) was amplified by PCR from 4 hr embryo cDNA, cut with XbaI, and inserted into AvrII and NheI sites sequentially in *pGEM-WIZ* (*pGEM-hibris-IR*). The inverted repeat was cut by XhoI/XbaI and inserted into pUAST transformation vector. *roughest RNAi* construct *pUAS-roughest-IR* was similarly constructed using *roughest* cDNA fragment 87–579. Transgenic lines were established by standard P element-mediated transformation methods. Four independent *UAS-hibris-IR* transformant lines were isolated: lines A102B1 and B203B2 on the X chromosome and lines A102A2 and B207A2 on the second chromosome. All gave similar rough eye phenotypes when crossed together with a *GMR-Gal4* driver. Except where noted, all figures were generated by two copies of transgenes *UAS-hibris-IR[B203B2]/+;UAS-hibris-IR[B207A2]/+*. For *UAS-roughest-IR*, three lines were isolated: lines D203A1 and D207A2 on the second chromosome and line E101B1 on the third chromosome. All gave similar rough eye phenotypes when driven by GMR-GAL4, and all figures were generated by two copies of transgenes *UAS-roughest-IR[D203A1]/+*; *UAS-roughest-IR[E101B1]/+* unless otherwise noted.

Quantitative RT-PCR

Total RNA was isolated from wild-type and *actin5C-Gal4/UAS-hibris-IR* third instar larvae using Trizol reagent (GIBCO-BRL). Real-time RT-PCR was performed in Mx3000P (Stratagene) using Absolute QPCR SYBR Green mix (ABgene) with the following primers: q-hbs101-F(TGAAGCCAGGAGCAACCTACTACT) and q-hbs101-R (ACTTGATATCGGGCA-TGAATTTACT) for *hibris*; q-rst204-F (CAG CGTGGTGTC-CCTAACCT) and q-rst204-R (CAGCCGTCTCATTGC TCACA) for *roughest*; and q-rp49-102F (GGCCCAAGATC-GTGAA GAAG) and q-rp49-102R (CCGATGT-TGGGCATCAGATAC) for the internal control *rp49*. Melting curve analysis showed a single peak for all samples. mRNA levels were assayed from three independent isolates. Average was approximately 49.5% reduction of *hibris* mRNA in Actin5C-Gal4/*UAS-hibris-IR* and 46.8% reduction of *roughest* transcript in *Actin5C-Gal4/UAS-roughest-IR* compared with wild-type.

Clonal Analysis

Clones overexpressing a transgene were induced at 18 hr APF, unless otherwise noted, by 30 min heat shock at 37°C in pupae of the following genotypes: *ywhsFlp/+;Act5C>y+>GAL4 UAS-GFP/UAS-hibris* (Figures 4E and 5E); *ywhsFlp/+;Act5C>y+>GAL4 UAS-GFP/UAS-roughest* (Figures 6A and 6B); *ywhsFlp/+;Act5C>y+>GAL4 UAS-GFP/UAS-hibris-IR* (Figure 4D); and *ywhsFlp/+;Act5C>y+>GAL4 UAS-GFP/UAS-roughest-IR*.

Excision of FLP-out cassette by FLPase led to GAL4-mediated expression of the transgene; clones were marked by GFP (Ito et al., 1997). To analyze the effect of targeted *roughest-IR* expression in the eye, FLP-out clones were induced at 3 hr APF and pupal eyes were dissected at 42 hr APF.

Immunostaining and In Situ Hybridization

Pupal eyes were dissected in PBS, fixed in 4% paraformaldehyde (PFA) in PBS, washed in PAXD (PBS containing 1% BSA, 0.3% Tri-

ton X-100, and 0.3% deoxycholate), and incubated with primary antibodies in PAXDG (PAXD containing 5% goat serum), followed by washing and incubation with secondary antibodies in PAXDG. Tissues were mounted in Vectashield mounting media (Vector Labs). Primary antibodies: mouse anti-Roughest Mab24A5.1 (1:100) (Schneider et al., 1995) and rabbit anti-lacZ (1:2000; 5 Prime→3 Prime). Rat anti-DE-cadherin (1:20), mouse anti-Armadillo (1:10), and mouse anti-Cut (1:10) were from Developmental Studies Hybridoma Bank at the University of Iowa. Secondary Alexa488 and Alexa568-conjugated anti-mouse, anti-rat, and anti-rabbit antibodies were used (1:1000; Molecular Probes).

Whole-mount in situ hybridization was carried out as described by Lehmann and Tautz (1994) with some modification for the pupal eye. Briefly, Dig-labeled antisense RNA probe was synthesized with the entire coding region of *roughest*. Pupal eyes were dissected in PBS and fixed in 4% PFA. After brief washing in PBT (PBS containing 0.1% Tween-20), the eyes were prehybridized with Hyb-A (50% formamide, 2×SSC, 5 mM EDTA, 50 μg/ml yeast tRNA, 0.2% Tween-20, 5 mg/ml Chaps, and 100 μg/ml Heparin) at 56°C, followed by hybridization with riboprobe in Hyb-A at 56°C. After washing in Hyb-B (50% formamide and 2×SSC), washing buffer was changed stepwise to PBT and tissues were incubated with anti-Dig-alkaline phosphatase (Roche, 1:5000). Chromogenic reaction was performed using BCIP/NBT (Roche) following manufacturer's instruction. Finally, tissues were dehydrated and mounted in aqueous/dry-mounting medium (Biomeda).

Cell Transfection and Coimmunoprecipitation

S2 cells were cultured and routinely maintained at 27°C in a spinner flask in Schneider medium with 10% FBS. Before transfection, cells were split into 6-well plates and allowed to attach for 12 hr. S2 cells were then transfected with each construct separately by the use of Cellfectin (Invitrogen). Constructs used were: *CaSpeR-hs-roughest-flag* (Roughest, FLAG-tagged), *CaSpeR-hs-roughest-V5* (Roughest, V5-tagged), *CaSpeR-hs-hibris-flag* (Hibris, FLAG-tagged), *CaSpeR-hs-hibris-V5* (Hibris, V5-tagged), *CaSpeR-hs sns-flag* (Sns, FLAG-tagged), and *CaSpeR-hs-sns-V5* (Sns, V5-tagged). To make these constructs, full-length *roughest*, *hibris*, or *sns* cDNA clones (Bour et al., 2000; Dworak et al., 2001; Ramos et al., 1993) were subcloned into *pGEM-T*, where FLAG or V5 was added to the C terminus. Each tagged gene was then shuttled into *CaSpeR-hs*. At 36 hr after transfection, cells were heat shocked twice at 37°C, 30 min each with 30 min break between. Cells were then resuspended in Schneider medium and cocultured by mixing two cell populations in a 1.5 ml eppendorf tube with rotation for 30 min at room temperature. Cells were then lysed in prechilled lysis buffer (5 mM EDTA, 0.5% Triton X-100, 150 mM NaCl, 1× protease inhibitor cocktail, and 50 mM Tris [pH 8.0]) for 1 hr at 4°C with rotation.

Immunoprecipitations were performed using mouse anti-FLAG M2 agarose (Sigma) or mouse anti-V5 agarose (Sigma) at 4°C overnight, followed by washing three times with lysis buffer. Precipitated proteins were resolved by SDS-PAGE, transferred to Nitrocellulose membrane, and probed with primary antibodies. Primary antibodies used for Western blot were: mouse anti-flag M2 (1:3000; Sigma) and mouse anti-V5 (1:5000; Invitrogen). The secondary antibodies were goat anti-mouse IgG-HRP (1:5000; Cell Signaling).

Supplemental Data

Supplemental Data include one figure and can be found with this article online at http://www.developmentalcell.com/cgi/content/full/8/6/925/DC1/.

Acknowledgments

We are grateful to Mary Baylies, Heather A. Dworak, and Helen Sink for flies and reagents. We thank Richard Carthew, Takashi Hayashi, Raphael Kopan, Junyang Lou, Brian Pierchala, Mal Steinberg, and members of our laboratory for helpful discussion and comments; Dennis Poehling for technical assistance; and Xinhui Li for advice. We also thank Yumi Kasai for help in quantitative RT-PCR. This project was supported by NIH-R01EY11495.

Received: September 3, 2004
Revised: January 25, 2005
Accepted: March 16, 2005
Published: June 6, 2005

References

Artero, R.D., Castanon, I., and Baylies, M.K. (2001). The immunoglobulin-like protein Hibris functions as a dose-dependent regulator of myoblast fusion and is differentially controlled by Ras and Notch signaling. Development *128*, 4251–4264.

Barclay, A.N. (2003). Membrane proteins with immunoglobulin-like domains—a master superfamily of interaction molecules. Semin. Immunol. *15*, 215–223.

Barletta, G.M., Kovari, I.A., Verma, R.K., Kerjaschki, D., and Holzman, L.B. (2003). Nephrin and Neph1 co-localize at the podocyte foot process intercellular junction and form cis hetero-oligomers. J. Biol. Chem. *278*, 19266–19271.

Basler, K., and Struhl, G. (1994). Compartment boundaries and the control of *Drosophila* limb pattern by hedgehog protein. Nature *368*, 208–214.

Boschert, U., Ramos, R.G., Tix, S., Technau, G.M., and Fischbach, K.F. (1990). Genetic and developmental analysis of irreC, a genetic function required for optic chiasm formation in *Drosophila*. J. Neurogenet. *6*, 153–171.

Bour, B.A., Chakravarti, M., West, J.M., and Abmayr, S.M. (2000). *Drosophila* SNS, a member of the immunoglobulin superfamily that is essential for myoblast fusion. Genes Dev. *14*, 1498–1511.

Cagan, R.L., and Ready, D.F. (1989). The emergence of order in the *Drosophila* pupal retina. Dev. Biol. *136*, 346–362.

Creighton, T.E. (1984). Proteins: Structures and Molecular Principles (New York: W.H. Freeman and Company).

Donoviel, D.B., Freed, D.D., Vogel, H., Potter, D.G., Hawkins, E., Barrish, J.P., Mathur, B.N., Turner, C.A., Geske, R., Montgomery, C.A., et al. (2001). Proteinuria and perinatal lethality in mice lacking NEPH1, a novel protein with homology to NEPHRIN. Mol. Cell. Biol. *21*, 4829–4836.

Dworak, H.A., Charles, M.A., Pellerano, L.B., and Sink, H. (2001). Characterization of *Drosophila hibris*, a gene related to human nephrin. Development *128*, 4265–4276.

Frohlich, A. (2001). A scanning electron-microscopic study of apical contacts in the eye during postembryonic development of *Drosophila melanogaster*. Cell Tissue Res. *303*, 117–128.

Garcia-Bellido, A., and Merriam, J.R. (1969). Cell lineage of the imaginal discs in *Drosophila* gynandromorphs. J. Exp. Zool. *170*, 61–75.

Gerke, P., Huber, T.B., Sellin, L., Benzing, T., and Walz, G. (2003). Homodimerization and heterodimerization of the glomerular podocyte proteins nephrin and NEPH1. J. Am. Soc. Nephrol. *14*, 918–926.

Hayashi, T., and Carthew, R. (2004). Surface mechanics mediate pattern formation in the developing retina. Nature *431*, 647–652.

Holtfreter, J. (1939). Gewebeaffinitat, ein Mittel der embryonal Formbildung. Arch Exp Zellforsch Gewebezucht *23*, 169–209.

Holtfreter, J. (1944). A study of the mechanics of gastrulation: part II. J. Exp. Zool. *95*, 171–212.

Hynes, R.O., and Lander, A.D. (1992). Contact and adhesive specificities in the associations, migrations, and targeting of cells and axons. Cell *68*, 303–322.

Ito, K., Awano, W., Suzuki, K., Hiromi, Y., and Yamamoto, D. (1997). The *Drosophila* mushroom body is a quadruple structure of clonal units each of which contains a virtually identical set of neurones and glial cells. Development *124*, 761–771.

Janody, F., Martirosyan, Z., Benlali, A., and Treisman, J.E. (2003). Two subunits of the *Drosophila* mediator complex act together to control cell affinity. Development *130*, 3691–3701.

Khoshnoodi, J., Sigmundsson, K., Ofverstedt, L.G., Skoglund, U., Obrink, B., Wartiovaara, J., and Tryggvason, K. (2003). Nephrin pro-

motes cell-cell adhesion through homophilic interactions. Am. J. Pathol. *163*, 2337–2346.

Lee, Y.S., and Carthew, R.W. (2003). Making a better RNAi vector for *Drosophila*: use of intron spacers. Methods *30*, 322–329.

Lehmann, R., and Tautz, D. (1994). In situ hybridization to RNA. Methods Cell Biol. *44*, 575–598.

Liu, G., Kaw, B., Kurfis, J., Rahmanuddin, S., Kanwar, Y.S., and Chugh, S.S. (2003). Neph1 and nephrin interaction in the slit diaphragm is an important determinant of glomerular permeability. J. Clin. Invest. *112*, 209–221.

Milan, M., Weihe, U., Perez, L., and Cohen, S.M. (2001). The LRR proteins capricious and Tartan mediate cell interactions during DV boundary formation in the *Drosophila* wing. Cell *106*, 785–794.

Miller, D.T., and Cagan, R.L. (1998). Local induction of patterning and programmed cell death in the developing *Drosophila* retina. Development *125*, 2327–2335.

Moses, K., and Rubin, G.M. (1991). Glass encodes a site-specific DNA-binding protein that is regulated in response to positional signals in the developing *Drosophila* eye. Genes Dev. *5*, 583–593.

Ramos, R.G., Igloi, G.L., Lichte, B., Baumann, U., Maier, D., Schneider, T., Brandstatter, J.H., Frohlich, A., and Fischbach, K.F. (1993). The irregular chiasm C-roughest locus of *Drosophila*, which affects axonal projections and programmed cell death, encodes a novel immunoglobulin-like protein. Genes Dev. *7*, 2533–2547.

Ready, D.F. (1989). A multifaceted approach to neural development. Trends Neurosci. *12*, 102–110.

Reiter, C., Schimansky, T., Nie, Z., and Fischbach, K.F. (1996). Reorganization of membrane contacts prior to apoptosis in the *Drosophila* retina: the role of the IrreC-rst protein. Development *122*, 1931–1940.

Rusconi, J.C., Hays, R., and Cagan, R.L. (2000). Programmed cell death and patterning in *Drosophila*. Cell Death Differ. *7*, 1063–1070.

Sanson, B., White, P., and Vincent, J.P. (1996). Uncoupling cadherin-based adhesion from wingless signalling in *Drosophila*. Nature *383*, 627–630.

Schneider, T., Reiter, C., Eule, E., Bader, B., Lichte, B., Nie, Z., Schimansky, T., Ramos, R.G., and Fischbach, K.F. (1995). Restricted expression of the irreC-rst protein is required for normal axonal projections of columnar visual neurons. Neuron *15*, 259–271.

Schock, F., and Perrimon, N. (2002). Molecular mechanisms of epithelial morphogenesis. Annu. Rev. Cell Dev. Biol. *18*, 463–493.

Sellin, L., Huber, T.B., Gerke, P., Quack, I., Pavenstadt, H., and Walz, G. (2003). NEPH1 defines a novel family of podocin interacting proteins. FASEB J. *17*, 115–117.

Shen, K., and Bargmann, C.I. (2003). The immunoglobulin superfamily protein SYG-1 determines the location of specific synapses in *C. elegans*. Cell *112*, 619–630.

Shen, K., Fetter, R.D., and Bargmann, C.I. (2004). Synaptic specificity is generated by the synaptic guidepost protein SYG-2 and its receptor, SYG-1. Cell *116*, 869–881.

Steinberg, M.S. (1963). Reconstruction of tissues by dissociated cells. Some morphogenetic tissue movements and the sorting out of embryonic cells may have a common explanation. Science *141*, 401–408.

Steinberg, M.S. (1970). Does differential adhesion govern self-assembly processes in histogenesis? Equilibrium configurations and the emergence of a hierarchy among populations of embryonic cells. J. Exp. Zool. *173*, 395–433.

Steinberg, M.S., and Takeichi, M. (1994). Experimental specification of cell sorting, tissue spreading, and specific spatial patterning by quantitative differences in cadherin expression. Proc. Natl. Acad. Sci. USA *91*, 206–209.

Strunkelnberg, M., Bonengel, B., Moda, L.M., Hertenstein, A., de Couet, H.G., Ramos, R.G., and Fischbach, K.F. (2001). rst and its paralogue kirre act redundantly during embryonic muscle development in *Drosophila*. Development *128*, 4229–4239.

Wolff, T., and Ready, D.F. (1991). Cell death in normal and rough eye mutants of *Drosophila*. Development *113*, 825–839.